IEEE Access
Multidisciplinary | Rapid Review | Open Access Journal

Received December 28, 2019, accepted January 13, 2020, date of publication January 17, 2020, date of current version January 27, 2020.

Digital Object Identifier 10.1109/ACCESS.2020.2967122

A Novel Inverter-Side Current Control Method of *LCL*-Filtered Inverters Based on High-Pass-Filtered Capacitor Voltage Feedforward

XINGDA ZHOU, (Student Member, IEEE), AND SHUAI LU, (Member, IEEE)
School of Electrical Engineering, Chongqing University, Chongqing 400044, China
Corresponding author: Shuai Lu (Lushuai1975@gmail.com)

ABSTRACT *LCL* filters have been widely used as the interface between inverters and power grids, but damping methods must be taken to solve the resonance of *LCL* filters. Considering overcurrent protection and inherent active damping, this paper focuses on the inverter-side current feedback (ICF) control. Some literatures have proposed that the capacitor voltage feedforward (CVF) is beneficial to the stability of the ICF control. However, in practical applications, it is found that the ICF control with CVF mainly faces two problems. Firstly, the CVF can be seen as a positive feedback loop, and it tends to cause low-frequency oscillation, especially in weak grid. Secondly, low-frequency harmonics in the grid voltage can easily distort the grid-side current of the inverter, even though the inverter-side current has been regulated well. In order to solve these two problems simultaneously, this paper proposes a novel inverter-side current control method, which adds a high-pass filter into the CVF path. In this paper, the design process of the high-pass filter parameters is analyzed, and the specific voltage feedforward structure of the proposed method to avoid the inverter startup inrush current is also discussed in detail. Simulations in MATLAB/SIMULINK and experiments based on a 6.6 kW prototype have been utilized to verify the effectiveness of the proposed method.

INDEX TERMS *LCL* filters, inverter-side current feedback, capacitor voltage feedforward, low-frequency oscillation, weak grid, high-pass filter.

I. INTRODUCTION

Grid-tied inverters are the main devices to connect renewable energy resources to the power grids [1]. In order to attenuate high-frequency harmonics caused by the pulse width modulation (PWM) inverters, a low-pass power filter is often needed. *LCL* filters are more competitive compared with *L* filters because of smaller volume and better attenuation capability. However, *LCL* filters tend to cause resonance problem without proper damping [2].

Damping methods of *LCL* filters can be classified into passive damping and active damping. A resistor in series with the capacitor is a common passive damping method of *LCL* filters [3]. But passive damping causes energy loss and weakens the suppression of high-frequency harmonics. Among the active damping methods, single-variable-feedback control only needs to sample the control target variable, such as the grid-side current [4]–[6] or the inverter-side current [7]–[9], so that it is competitive in industrial applications because no additional sensors are required. Moreover, the inverter-side current single-loop feedback control has an inherent damping effect [7], and the inverter-side current can be also used for overcurrent protection. So this paper mainly focuses on the inverter-side current feedback (ICF) control.

Recently, the effect of the capacitor voltage feedforward (CVF) on the ICF control has been researched in many papers. It is reported that the third-order *LCL* filter can be simplified to a first-order *L* filter when the CVF is used [10], [11], and the CVF can also improve the robustness of *LCL* active damping against the grid impedance for the ICF control [12]–[15]. However, although the CVF is helpful for the active damping of the *LCL* filter at the resonant frequency, the voltage feedforward loop is detrimental to the current control in low-frequency range, especially in weak grids [16], [17]. In [18], it is found that if the voltage feedforward coefficient is too large, the low-frequency

The associate editor coordinating the review of this manuscript and approving it for publication was Alfeu J. Sguarezi Filho.

instability of current control will be caused. In order to resolve this contradiction, this paper proposes to add a high-pass filter (HPF) into the CVF loop. On the one hand, the high-frequency component of the capacitor voltage can still pass the HPF, which can continue to guarantee the damping of the ICF control. On the other hand, in the low-frequency range, the influence of the CVF can be mitigated. Therefore, by selecting the parameters of the HPF carefully, the active damping of the *LCL* filter is guaranteed, and low-frequency oscillation caused by the voltage feedforward can be also prevented.

Besides, the method of HPF CVF can also solve the problem of the grid low-frequency harmonic distortion for the ICF control of grid-tied inverters. Because the control target of the ICF control is not the grid-side current, the low-frequency harmonics in the grid voltage can generate corresponding harmonic currents flowing through the capacitor freely [19]. To overcome this problem, the capacitor current is sampled by a current sensor as a feedforward part of the inverter-side current reference command in [20]. Similarly, to save the extra current sensor, [21] uses a precise digital differentiator to obtain the capacitor current from the capacitor voltage. However, this kind of method is equivalent to the grid-side current feedback control, and changes the original stability characteristics of the ICF control. Actually, the grid voltage feedforward is the most direct way to reduce the influence of the grid low-frequency harmonics [22], but it is a little bit different in the case of ICF control. In [23], [24], a complete point of common coupling (PCC) voltage feedforward form is deduced to suppress the grid voltage harmonics, but the feedforward form includes a first-order derivative and a second-order derivative, which are difficult to realize in digital domain. In this paper, a simple HPF is added into the CVF loop, and it is not as accurate as the method in [23], [24], but it can also reduce the grid voltage low-frequency harmonic pollution of the ICF control effectively.

The organization of this paper is shown as follows: a mathematic model of the ICF control with HPF CVF is established in section II. Section III discusses the stability of the proposed method. The grid voltage harmonic attenuation capability of the proposed method is analyzed in Section IV. A complete ICF control implementation structure and simulation results are shown in Section V. Section VI includes the experiment results based on a 6.6 kW grid-tied inverter prototype. The conclusion is made in section VII.

II. MATHEMATICAL MODEL AND PROPOSED METHOD

A typical grid-tied inverter interfaced with a *LCL* filter is shown in Fig. 1, where L_1, L_2, C_f are the inverter-side inductor, grid-side inductor and capacitor of the *LCL* filter, and L_g represents the grid inductive impedance or the leakage inductance of a transformer.

The parameters of the grid-tied inverter used in this paper is shown in Table 1. Single sampling is used in this paper, so the sampling frequency and switching frequency are the same. In this paper, the inverter-side currents are sampled for the feedback control, and the capacitor voltages are sampled for the feedforward and the grid voltage phase synchronization.

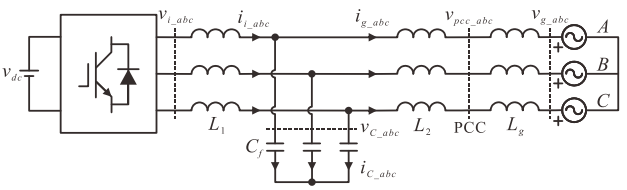

FIGURE 1. Grid-tied inverter interfaced with a *LCL* filter.

TABLE 1. Parameters of the grid-tied inverter.

Symbol	Description	Value
L_2	Grid-side inductance	190 μH
C_f	*LCL* filter capacitance	30 μF
L_1	Inverter-side inductance	400 μH
f_s	Sampling frequency	12 kHz
f_{sw}	Switching frequency	12 kHz
f_0	Grid frequency	50 Hz

Applying Kirchhoff's laws and Laplace transform to Fig. 1, the mathematic model of the system in frequency domain can be expressed by

$$\begin{aligned} v_{i\_abc}(s) &= sL_1 i_{i\_abc}(s) + v_{C\_abc}(s) \\ v_{C\_abc}(s) &= sL_T i_{g\_abc}(s) + v_{g\_abc}(s) \\ i_{i\_abc}(s) &= sC_f v_{C\_abc}(s) + i_{g\_abc}(s) \\ L_T &= L_g + L_2 \end{aligned} \tag{1}$$

where v_{i_abc} and i_{i_abc} are the output phase voltages and currents of the inverter; v_{g_abc} and i_{g_abc} are the grid phase voltages and currents; v_{c_abc} and i_{c_abc} are the voltages and currents of C_f respectively. L_T is the sum of the grid-side inductance L_2 and the grid inductance L_g. A stationary $\alpha\beta$ reference frame is adopted in this paper. Equation (2) can be obtained from (1) through Clarke transform.

$$\begin{aligned} v_{i\_\alpha\beta}(s) &= sL_1 i_{i\_\alpha\beta}(s) + v_{C\_\alpha\beta}(s) \\ v_{C\_\alpha\beta}(s) &= sL_T i_{g\_\alpha\beta}(s) + v_{g\_\alpha\beta}(s) \\ i_{i\_\alpha\beta}(s) &= sC_f v_{C\_\alpha\beta}(s) + i_{g\_\alpha\beta}(s) \end{aligned} \tag{2}$$

Therefore, the transfer function diagram of the ICF control with CVF is shown in Fig. 2, where $G_c(z)$ is the discrete inverter-side current controller; $G_{vf}(z)$ is added into the CVF loop; z^{-1} represents one cycle computation digital delay; zero-order holder (ZOH) represents the PWM modulation. It should be noticed that the grid voltage v_g in Fig. 2 may also contain low-frequency harmonics, in addition to the fundamental frequency component.

The most common CVF form is the unit voltage feedforward, where $G_{vf}(z) = 1$. However, as mentioned in Section I, the unit CVF has bad dynamic performance in weak grid, and does not have a good attenuation capability of the low-frequency grid voltage harmonics. So this paper proposed a HPF added into the CVF loop, and the expression of the HPF in frequency domain is shown in (3), where H and ω_c

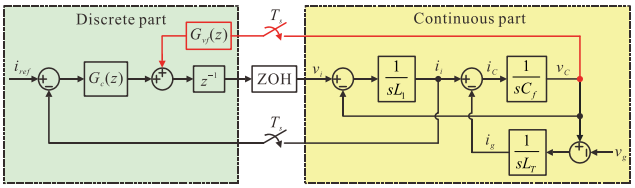

FIGURE 2. Transfer function diagram of the system.

are the gain coefficient and cut-off frequency of the HPF.

$$G_{vf}(s) = \frac{Hs}{s + \omega_c} \tag{3}$$

According to the discretization method of Tustin, the discrete expression of (3), can be derived as (4), where T_s is the control period.

$$G_{vf}(z) = \frac{2H(z-1)}{(\omega_c T_s + 2)z + (\omega_c T_s - 2)} \tag{4}$$

III. STABILITY ANALYSIS

The resonant frequency of the *LCL* filter is usually very high. So, the stability at the resonance frequency of the ICF control is very sensitive to digital delay. In order to ensure the correctness of the stability analysis, the accuracy of the system modeling in the high frequency region must be guaranteed. Therefore, the transfer function model of the system in Fig. 2 should be transformed into discrete domain as shown in Fig. 3, where the grid voltage v_g can be ignored temporarily.

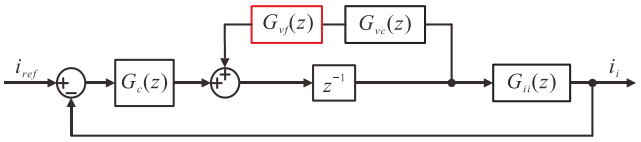

FIGURE 3. Simplified transfer function diagram of the system in discrete domain.

The continuous part in a hybrid system based on ZOH can be discretized precisely by the z-transform method in [25]. Therefore, the discrete transfer functions $G_{ii}(z)$ and $G_{vc}(z)$ in Fig. 3 can be deduced as

$$G_{ii}(z) = \frac{T_s}{(L_1 + L_T)(z-1)} + \frac{L_T}{\omega_{res} L_1 (L_1 + L_T)} \cdot \left(\frac{(z-1)\sin(\omega_{res} T_s)}{z^2 - 2z\cos(\omega_{res} T_s) + 1} \right) \tag{5}$$

$$G_{vc}(z) = \frac{L_T(z+1)[1 - \cos(\omega_{res} T_s)]}{(L_1 + L_T)[z^2 - 2z\cos(\omega_{res} T_s) + 1]} \tag{6}$$

where $\omega_{\text{res}} = 2\pi f_{\text{res}}$ is the resonance angular frequency of the *LCL* filer with consideration of the grid inductance, and ω_{res} is expressed by

$$\omega_{res} = \sqrt{\frac{L_1 + L_T}{L_1 L_T C_f}}. \tag{7}$$

The most direct way to judge the stability of the system in discrete domain is the pole plot of the closed-loop transfer function. The open-loop and closed-loop transfer functions of Fig. 3 are deduced as (8) and (9) respectively.

$$T_{ol}(z) = \frac{z^{-1} G_c(z) G_{ii}(z)}{1 - z^{-1} G_{vf}(z) G_{vc}(z)} \tag{8}$$

$$T_{cl}(z) = \frac{T_{ol}(z)}{1 + T_{ol}(z)} \tag{9}$$

First, the pole plots of the closed-loop transfer function $T_{cl}(z)$ of two different CVF forms are drawn in Fig. 4 based on the parameters in Table 1, where $G_c(z)$ is defined as a constant ($G_c(z) = 1.85$), and the grid inductance L_g changes sequentially from 0 to 2000 μH. In order to express the varied grid inductance in per unit, the inverter-side inductance of the *LCL* filter is selected as the reference, so that the grid inductance in per unit represented by L_{g_pu} can be expressed by the ratio of L_g to L_1. In Fig. 4, (a) represents the no CVF case ($G_{vf}(z) = 0$), and (b) represents the unit CVF case ($G_{vf}(z) = 1$), where L_{g_pu} increases from 0 to 5.

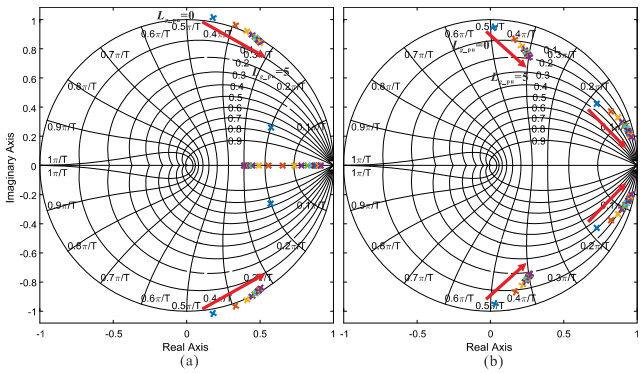

FIGURE 4. Pole plots of the ICF control closed-loop transfer function. (a) without CVF, (b) with unit CVF.

In Fig. 4 (a), it is obvious that in the absence of CVF, the ICF control loop is hardly stable, unless the grid inductance is very large. When the unit CVF is adopted in Fig. 4 (b), the stability of the system is greatly improved, and all the poles are within the unit circle. However, an interesting phenomenon can be seen from Fig. 4 (b). There are high-frequency and low-frequency poles in the pole plot of the closed-loop transfer function. In the case of the unit CVF, although the high-frequency poles are within the unit circle, the low-frequency poles are gradually moving to the edge of the unit circle as the grid inductance increases. That is to say, as the value of the grid inductance increases, the stability of the system in the low-frequency range is becoming worse (although the high-frequency stability becomes better).

So, it can be seen that the unit CVF shows a good active damping performance, but it is necessary to take measures to avoid the low-frequency oscillation when the grid inductance is large.

Actually, voltage feedforward is likely to cause low-frequency oscillation of the inverter output current in the

case of weak grid [18]. As shown in Fig. 4 (a), although the high-frequency poles are unstable, the low-frequency poles are in a very safe location. So, in order to maintain the advantage of the CVF in high-frequency range and eliminate the disadvantage in low-frequency range, we can add a HPF in the CVF loop.

There are two parameters ω_c and H of the HPF as shown in (4). In order to reduce the influence of the HPF on the high-frequency components and at the same time try to fully attenuate the low-frequency components in the CVF, the cut-off frequency ω_c of the HPF can be designed as (10), where $\omega_{\text{res\_min}}$ represents the minimum resonance frequency of the *LCL* filter considering the grid inductance L_g, and $\omega_{\text{res\_min}}$ can be calculated from (11). Based on the parameters in Table 1 and supposing $L_{g_max} = 800\ \mu$H, ω_c can be determined as 6280 rad/s.

$$0.5\omega_{res\_\min} \le \omega_c \le 0.7\omega_{res\_\min} \tag{10}$$

$$\omega_{res\_\min} = \sqrt{\frac{L_1 + (L_1 + L_{g\_\max})}{L_1(L_1 + L_{g\_\max})C_f}} \tag{11}$$

As for the parameter H in (4), too high H causes low-frequency oscillations, and too small H causes insufficient high-frequency *LCL* resonance damping, so the final value of H can be determined by the pole plots under actual parameters. The pole plots of the $T_{cl}(z)$ with different H when the HPF CVF is adopted are shown in Fig. 5, and the other parameters in Fig. 5 are the same as Fig. 4.

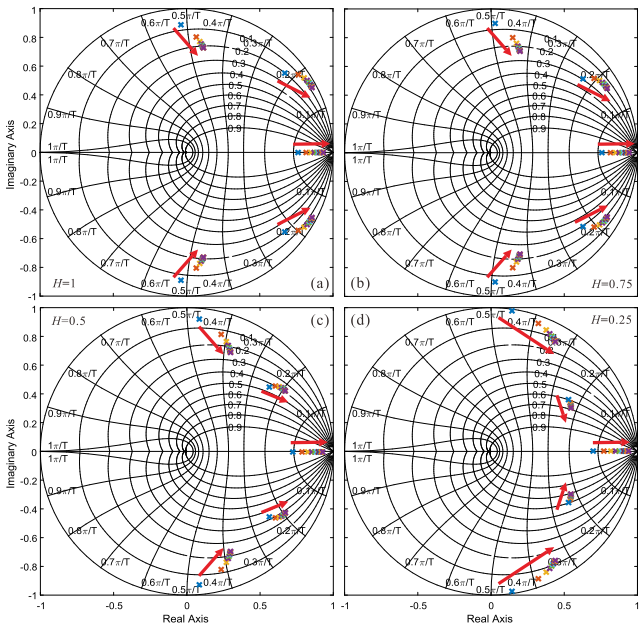

FIGURE 5. Pole plots of the ICF control closed-loop transfer function with HPF CVF. (a) $H = 1$, (b) $H = 0.75$, (c) $H = 0.5$, (d) $H = 0.25$.

From Fig. 5 (a) to (d), a suitable value of H is 0.5, which can guarantee a good stable margin in both low and high frequency range. The design process of the HPF parameters here is only by simply observing the MATLAB plots. In the appendix section, an optimal HPF parameter design method based on MATLAB program is provided.

Finally, comparing Fig. 4 and Fig. 5 (c), it is obvious that the HPF CVF can not only ensure effective damping at the resonance frequency of the *LCL* filter, but also avoid low-frequency oscillation in weak grid, which is a good method to kill two birds with one stone.

IV. GRID VOLTAGE HARMONIC SUPPRESSION

In practical three-phase applications, the grid voltage will contain some low-order harmonics, such as the 5th, 7th, 11th, 13th, 17th and 19th harmonics. These harmonics cannot be ignored, especially for the ICF control grid-tied inverters. Because the ICF control target is the inverter-side current, the harmonic currents generated by the grid voltage harmonics can flow freely though the *LCL* capacitors, resulting in severe harmonic pollution in the grid-side currents.

This section shows the research of the grid voltage harmonic attenuation capability of the proposed method, and the main object of the research is the low-order harmonics in the grid voltage, so the analysis process is not very sensitive to digital delay. Certainly, the discrete domain analysis can also be applied in this section, but a disadvantage of the discrete domain analysis method is that the discretization process of the transfer function is very complicated. In order to reduce complex derivation process and make this paper clearer, we decide to analyze in frequency domain in this section. So Fig. 2 can be simplified as Fig. 6, where assuming $I_{ref} = 0$. It must be noticed that the transfer function $G_d(s)$ in Fig. 6 represents the computation and ZOH delay, and cannot be ignored, otherwise, there will be mistakes during the derivation process. $G_d(s)$ can be expressed by (12) according to the Pade approximant, where $T_d = 1.5\ T_s$.

$$G_d(s) \approx \frac{1 - \frac{T_d s}{2} + \frac{(T_d s)^2}{12}}{1 + \frac{T_d s}{2} + \frac{(T_d s)^2}{12}} \tag{12}$$

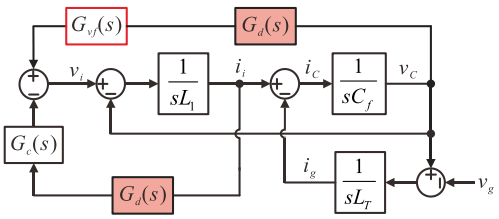

FIGURE 6. Transfer function diagram of the system in frequency domain when $I_{ref} = 0$.

Based on Fig. 6, the transfer function $G_{vgig}(s)$ from v_g to i_g can be derived as (13).

$$G_{vgig}(s) = \frac{i_g(s)}{v_g(s)} = \frac{1}{\frac{1}{\frac{G_{vf}(s)G_d(s)-1}{sL_1+G_c(s)G_d(s)} - sC_f} - sL_T} \tag{13}$$

Before discussing the attenuation capability of $G_{vgig}(s)$, it is necessary to illustrate the form of the current controller $G_c(s)$, because $G_c(s)$ also has a relationship with (13).

As the stationary $\alpha\beta$ reference frame is adopted in this paper, a quasi-proportional-resonance (QPR) current controller is preferred. The design of the QPR controller is independent, because the QPR controller is near the fundamental frequency, and it almost does not affect the damping of the *LCL* resonance. The QPR controller applied to control the inverter-side current is shown as

$$G_c(s) = K_p + \frac{2K_r\omega_i s}{s^2 + 2\omega_i s + \omega_0^2} + K_{rh}\omega_i \sum_{h=5,7} \frac{s\cos(\varphi_h) - h\omega_0 \sin(\varphi_h)}{s^2 + 2\omega_i s + (h\omega_0)^2} \quad (14)$$

where K_p is the overall gain of $G_c(s)$; K_r is the fundamental frequency gain; ω_0 is the grid angle frequency. In practice, the grid frequency usually swings within 0.5 Hz ($= f_i$) from the standard value, so that ω_i can be selected as $\pi(= 2\pi f_i)$. In (14), h is the order of the harmonics that need to be suppressed; K_{rh} determines the gain at the harmonic frequency; φ_h is the phase angle that needs to be compensated. The reason for adding the 5th and 7th resonance controllers in $G_c(s)$ is to suppress the 5th and 7th harmonics in the grid voltage and to compensate for the zero-crossing distortion of the current waveform caused by the PWM dead zone. Based on the parameters in Table 1, all the parameters of $G_c(s)$ in (14) can be shown in Table 2.

TABLE 2. Parameters of the current controller.

Symbol	Description	Value
K_p	Overall gain	1.85
K_r	Fundamental frequency gain	60
K_{rh}	Harmonic frequency gain	150
φ_5	5th compensated phase angle	0.87 rad/s
φ_7	7th compensated phase angle	0.87 rad/s

So, all the parameters in (13) have been obtained (the parameters of the HPF are the same as Section III). In light of (13), there is an ideal situation: if $G_{vf}(s)$ satisfies the condition in (15), the harmonics of the grid voltage can be totally suppressed. But the condition in (15) includes a first-order derivative and a second-order derivative, which is impractical in digital control system.

$$\frac{G_{vf}(s)G_d(s) - 1}{sL_1 + G_c(s)G_d(s)} - sC_f = 0 \quad (15)$$

Similar conclusion as (15) has been put forward by [23], [24]. References [23], [24] mainly focuses on the capability to suppress grid voltage harmonics of the ICF control, and proposes a complete CVF method, where the form of $G_{vf}(s)$ is expressed as $(1+sG_c(s)C_f + s^2L_1C_f)$. In the real applications, the part of $s^2L_1C_f$ is often omitted, because the value of L_1C_f is very small and the second-order differential s^2 is not applicable in digital control. So, the complete CVF will be analyzed in the form of $(1+sG_c(s)C_f)$.

Fortunately, by adding a HPF in the CVF loop can reduce the influence of the grid voltage harmonics effectively too. It is a very simple method, but has a good performance. In order to clarify the effectiveness of the proposed method, the bode plots of $G_{vgig}(s)$ are drawn in Fig. 7 based on the parameters in Table 1 and 2.

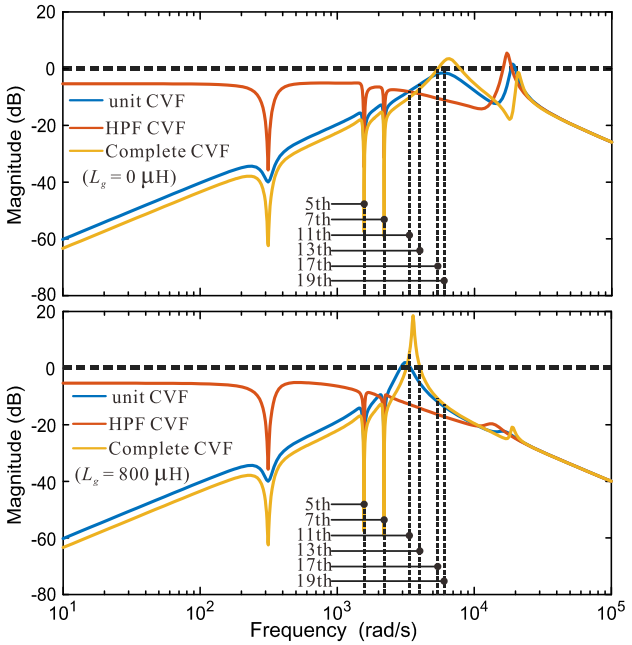

FIGURE 7. Bode plots of $G_{vgig}(s)$ under different CVF forms when $L_g = 0\mu$H and 800 μH.

In Fig. 7, two different values of L_g has been considered ($L_g = 0$ and 800 μH), and three different CVF forms are compared, and they are unit CVF, HPF CVF and complete CVF.

When $L_g = 0\mu$H, the unit CVF method shows a good attenuation of the grid voltage v_g in the low-frequency range below 350 Hz, but the attenuation capability becomes worse near 950 Hz, and there is an obvious resonance peak at the frequency of 950 Hz. In general, the largest value of this resonance peak is still under 0 dB line, so it still has a certain attenuation effect on the grid voltage harmonics. As for the HPF CVF method, this resonance peak at 950 Hz of $G_{vgig}(s)$ can be completely eliminated, so the HPF CVF has a better attenuation effect on 5th to 19th gird voltage harmonics compared with the unit CVF. However, in the frequency band below 350 Hz, the capability to suppress grid voltage harmonics of the HPF CVF is not very strong, but the 5th and 7th resonance controllers in $G_c(s)$ can compensate for this deficiency.

When $L_g = 800\mu$H, the attenuation capability of $G_{vgig}(s)$ on the grid voltage harmonics becomes weak when the unit CVF method is adopted. It can be seen that the resonance peak of $G_{vgig}(s)$ moves down to 550 Hz, and what is worse is that the ability to suppress grid voltage harmonics of the unit CVF is basically none, and it may even amplify the grid voltage harmonics. However, the HPF CVF shows a stable grid voltage harmonic attenuation capability, even in the case of large grid inductance.

From Fig. 7, It can be indeed seen that the complete CVF method proposed in [23], [24] has a better suppression effect on the grid voltage harmonics compared with unit CVF or HPF CVF in the low-frequency range. However, the complete CVF has the similar disadvantage (resonance peak) compared with the unit CVF, which can amplify grid voltage harmonics near certain frequencies. Moreover, [23] do not consider the stability of the ICF control under weak grids. The pole plots of the ICF control closed-loop transfer function under varied grid inductance with HPF CVF and complete CVF are compared in Fig. 8, where the first-order differential in the complete CVF is discretized by the method of Backward Euler. It is obvious that the poles of the complete CVF method gradually approaches the edge of the unit circle with the increase of the grid inductance, which indicates that the stability of the ICF control gradually weakens. So, the HPF CVF method proposed in this paper is more adaptable to weak grids.

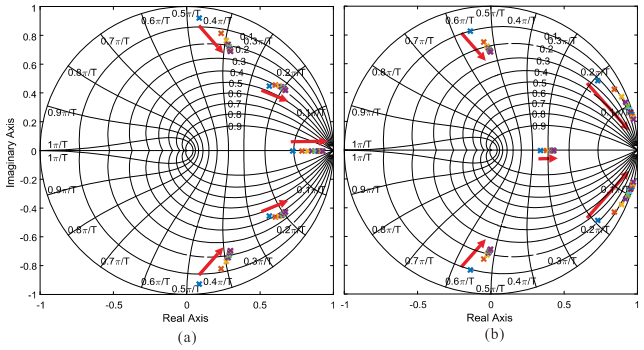

FIGURE 8. Pole plots of the ICF control closed-loop transfer function. (a) with HPF CVF, (b) with complete CVF.

Therefore, the HPF CVF method proposed in this paper can greatly improve the attenuation capability of the ICF control on the grid voltage harmonics, and the method is very simple to implement.

V. CONTROL FRAME AND SIMULATION RESULTS

A three-phase grid-tied two-level inverter simulation model based on MATLAB/SIMULINK is used to verify the controller design of the proposed method in this paper. The controller structure of the simulation model is shown in Fig. 9. In Fig. 9, one thing must be emphasized. The voltage feedforward has an another important function that is to prevent the inrush current when the inverter PWM starts. If the HPF CVF method is directly adopted, the low-frequency components in the capacitor voltage will be excessively attenuated, resulting in a small amplitude of the feedforward voltage, which will lead to the inrush current. So additional compensation measures must be taken to prevent the inverter starting inrush current. The method adopted in Fig. 9 is to divide the HPF CVF into two parts. The first part is the high-pass-filtered capacitor voltage, and the second part is the fundamental frequency component of the capacitor voltage. The fundamental frequency component can be obtained by

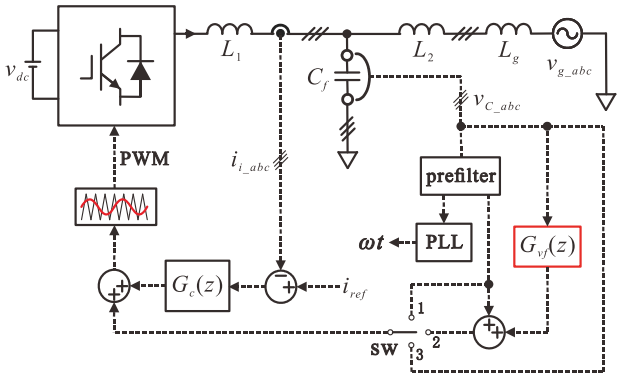

FIGURE 9. Controller structure of the simulation model.

the DDSRF-PLL [26]. The DDSRF-PLL can be seen as a PLL plus a prefilter as shown in Fig. 9. The capacitor voltage filtered by the prefilter can be approximately considered as a pure fundamental frequency component, which is only used for the prevention of the inrush current, and will not affect other characteristics of the ICF control. Therefore, according to the CVF structure in Fig. 9, when SW is at 1 position, it means no CVF; when SW is at 2 position, it means the HPF CVF; when SW is at 3 position, it means the unit CVF.

The hardware parameters of the simulation model are shown in TABLE 1, and the control parameters are shown in Table 2. In the simulation, the peak value of the grid phase voltage is 155 V, and the inverter dc-side voltage is 320 V. The dynamic process of the waveforms is recorded when the peak value of the current reference command steps from 0 A to 28 A.

To further illustrate the effectiveness of the voltage feedforward structure in Fig. 9, the inverter startup current simulation waveforms are shown in Fig. 10, where Fig. 10 (a) represents only using the high-pass-filtered capacitor voltage, and Fig. 10 (b) represents using the high-pass-filtered capacitor

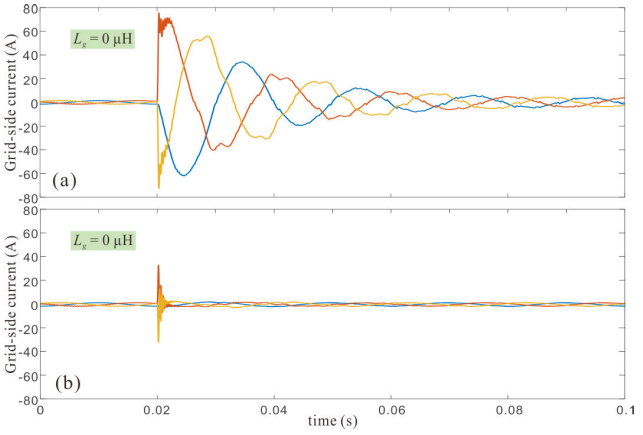

FIGURE 10. Inverter startup current simulation waveforms. (a) only using the high-pass-filtered capacitor voltage. (b) using the high-pass-filtered capacitor voltage and the fundamental frequency component of the capacitor voltage compensation.

voltage and the fundamental frequency component of the capacitor voltage compensation.

In Fig. 10, at the time of 0.02 s, the inverter control is started, and the current reference command is 0 A. It is obvious that if only the high-pass-filtered capacitor voltage is applied, there will be huge inrush currents (close to 80 A) at the moment of starting, which is very dangerous and impractical. However, if the voltage feedforward structure in Fig. 9 (SW is at 2 position) is adopted, the inrush current can be almost completely eliminated as shown in Fig. 10 (b).

In Fig. 11, the ICF control without CVF is tested when the grid inductance is 0 or 800 μH. It can be seen that when the CVF is removed, the ICF control cannot keep stable, regardless of the value of the grid inductance. But when $L_g = 800\mu$H, the current waveforms seems a little bit more stable, which is consistent with the analysis in Fig. 4 (a).

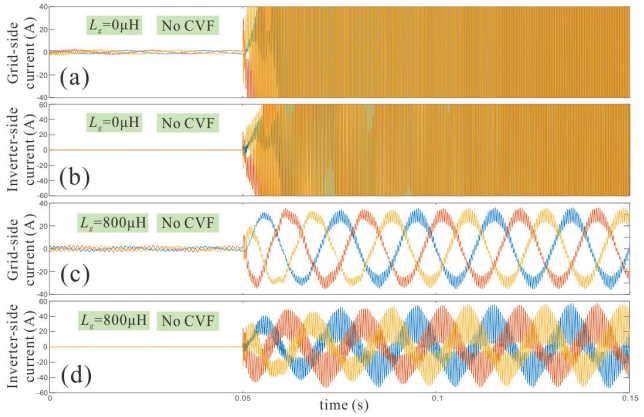

FIGURE 11. Simulation waveforms of the inverter-side and grid-side currents without CVF. (a) and (b) $L_g = 0$ μH. (c) and (d) $L_g = 800$ μH.

In Fig. 12 (a), the unit CVF is used in the ICF control. Comparing Fig. 11 (c) and Fig. 12 (a), the unit CVF improves the stability of the grid-side current significantly when $L_g = 800\mu$H. However, the unit CVF also brings another problem. When the inverter controller starts to work at 0.05 s

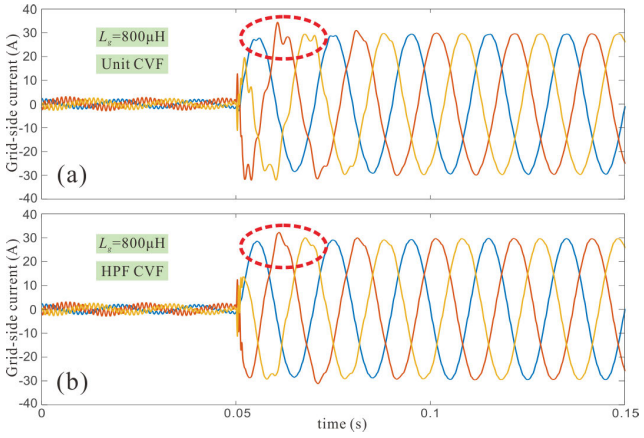

FIGURE 12. Simulation waveforms when $L_g = 800\mu$H. (a) unit CVF, (b) HPF CVF.

in Fig. 12 (a), there is an obvious oscillation process in the red circle, because the voltage feedforward tends to result in low-frequency oscillation in weak grid as shown in Fig. 4 (b). In order to solve this problem, the HPF CVF is adopted in Fig. 12 (b). It is clear from Fig. 12 (a) and (b) that the HPF CVF can effectively reduce the oscillation during the grid-side current step process, which is beneficial to the stability of the system.

To test the grid voltage harmonic attenuation capability of the proposed method, one percent 5th and 11th harmonic voltages are added into the grid voltage v_g in Fig. 13.

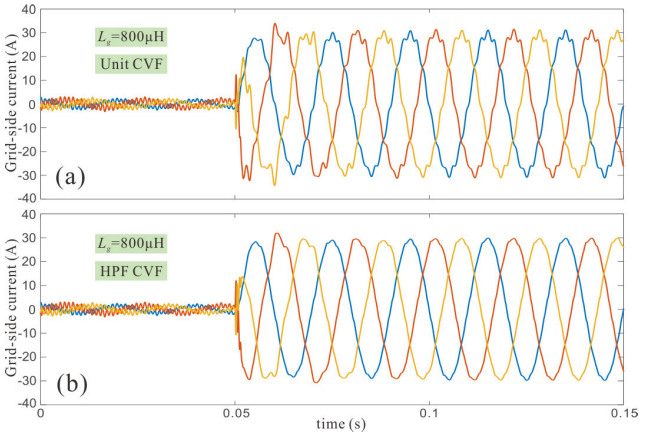

FIGURE 13. Simulation waveforms under distorted grid voltage when $L_g = 800\mu$H. (a) unit CVF, (b) HPF CVF.

It is obvious that there is serious harmonic pollution in the grid-side current in Fig. 13 (a) when the unit CVF are used, but when the HPF CVF method is used, the total harmonic distortion (THD) of the grid-side current is greatly reduced. Moreover, in Fig. 14, the fast Fourier transform (FFT) analysis is applied to the grid-side current simulation waveforms of Fig. 13. Fig. 14 (a) are the FFT results of the unit CVF method, and Fig. 14 (b) are the FFT results of the HPF CVF method. By using the method of HPF CVF, the THD of the grid-side current can be reduced from 5.55% to 1.74%, and the suppression of the 11th harmonic is particularly obvious. Therefore, the HPF CVF method can improve the grid voltage harmonic attenuation capability of the ICF control.

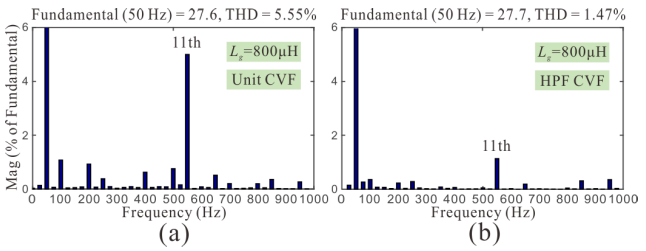

FIGURE 14. FFT analysis of the simulation waveforms under distorted grid voltage when $L_g = 800\mu$H. (a) unit CVF, (b) HPF CVF.

VI. EXPERIMENT RESULTS

In order to verify the effectiveness of the proposed method experimentally, a 6.6 kW three-phase grid-tied two-level inverter low-voltage prototype is utilized. The parameters of the prototype are also shown in TABLE 1. The experimental prototype is introduced in Fig. 15. The dc side of the inverter is supported by a programmable dc power supply, and the output current flows through an isolated transformer into the grid. In the experiment, the dc-side voltage is 320 V, the peak value of the grid phase voltage is 166.6 V, and the active power current of 28 A peak value is injected into the grid. For the inverter prototype, an 800 μH inductor is adopted to simulate the grid inductive impedance, and the leakage inductance of the isolated transformer is about 20 μH. The parameters of the controller $G_c(z)$ are the same as that have been achieved in section V.

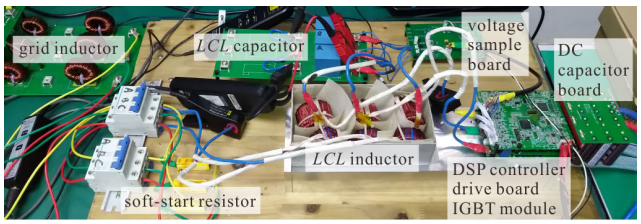

FIGURE 15. 6.6 kW Three-phase grid-tied two-level inverter prototype.

Firstly, the line voltage v_{g_ab} waveform of the grid voltage is recorded in Fig. 16, and there are obvious 5th, 7th, 11th, 17th and 19th harmonic voltages in v_{g_ab} through the FFT analysis. So it is very important to pay attention to the grid voltage harmonics suppression.

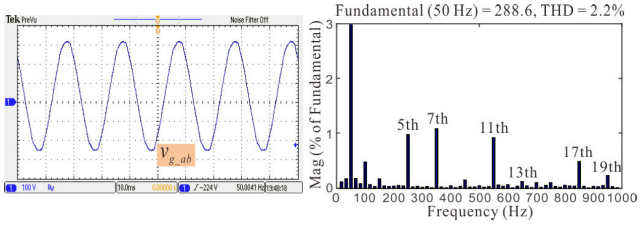

FIGURE 16. The waveform of the line voltage v_{g_ab} and its FFT analysis.

A. UNIT CAPACITOR VOLTAGE FEEDFORWARD

The experiment results of the unit CVF method is shown in Fig. 17, where channel 1 of the oscilloscope represents the waveform of the capacitor voltages v_{C_ab}, and the grid-side current i_{g_a} are recorded by channel 3. The experiment waveforms of the HPF CVF method in Fig. 18 are also recorded in the corresponding form.

In Fig. 17 (a), when the 800 μH grid inductor is not added to the prototype, the grid-side current i_{g_a} is almost normal. But some small high-frequency harmonics can still be observed. This phenomenon can be explained by Fig. 7. In Fig. 7, it can be seen that the unit CVF method does not have a good attenuation capability around 17th and

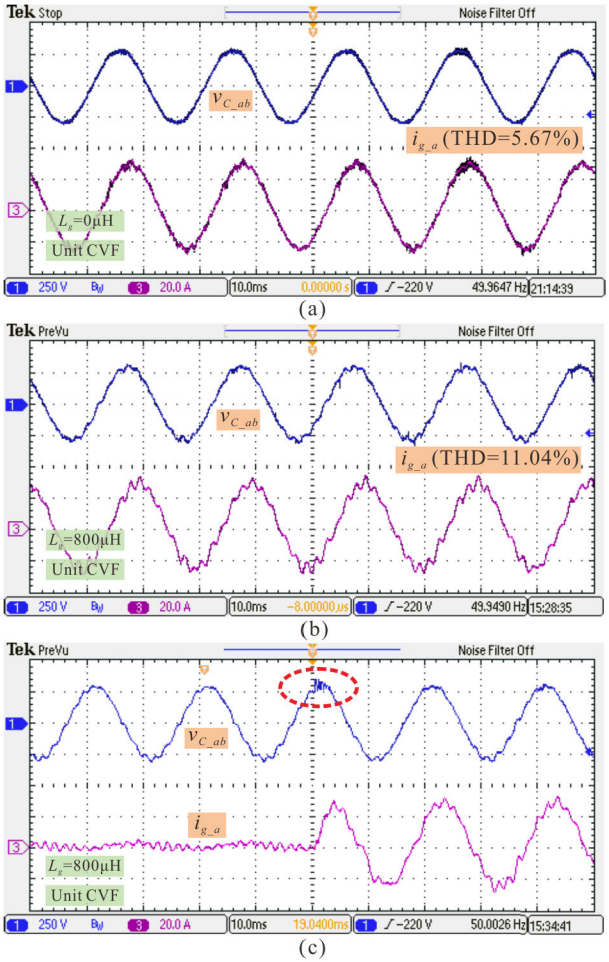

FIGURE 17. Experimental results with unit CVF. (a) $L_g = 0\mu$H, (b) and (c) $L_g = 800\mu$H.

19th harmonics, so the 17th and 19th harmonic voltages in v_{g_ab} can easily affect the waveforms of i_{g_a}. This situation becomes worse as shown in Fig. 17 (b) when $L_g = 800\mu$H, because the unit CVF almost cannot suppress the 11th and 13th harmonics of the grid voltage at all, so that there are obvious 11th harmonic current in i_{g_a}, which is similar as the simulation results in Fig. 13 (a). Besides, the dynamic performance is also tested during i_{g_a} steping from 0 A to 28 A when $L_g = 800\mu$H in Fig. 17 (c). Due to the interference of harmonic currents in i_{g_a}, it is difficult to distinguish the dynamic changes of i_{g_a}, but the dynamic performance can be seen from the capacitor voltage v_{C_ab}, and the dynamic performance of the ICF control seems not very good, because a little bit large oscillation appears in v_{C_ab} during the current step.

B. HPF CAPACITOR VOLTAGE FEEDFORWARD

Fig. 18 (a) and (b) are the steady-state waveforms when using the HPF CVF method under $L_g = 0$ and 800 μH respectively. It can be seen that no matter whether $L_g = 0$ or 800 μH, the grid-side current i_{g_a} can maintain a good fundamental frequency sine waveform, and the THD of i_{g_a} is much lower

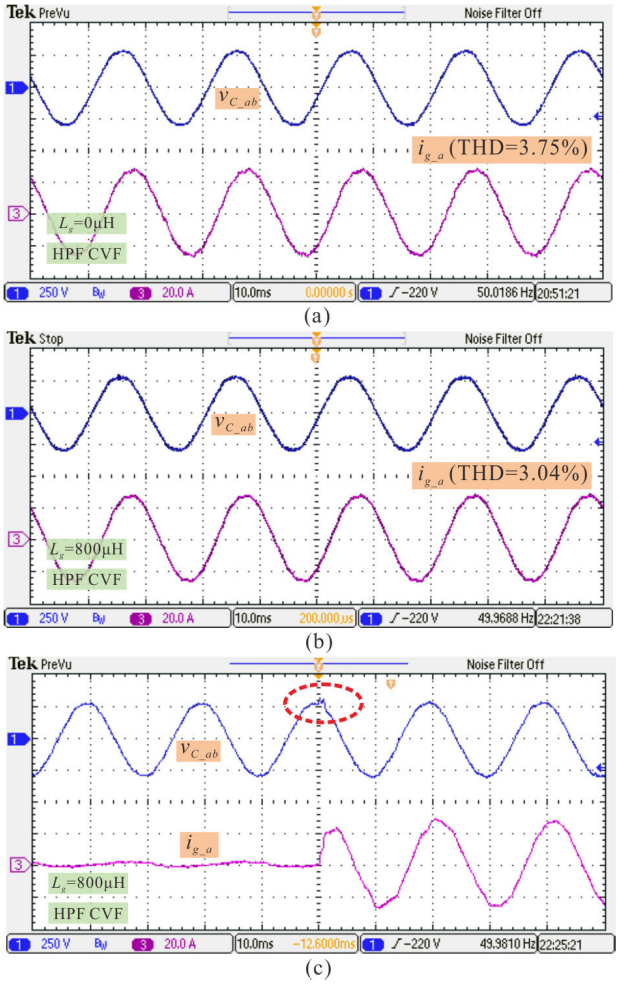

FIGURE 18. Experimental results with HPF CVF. (a) $L_g = 0\mu$H, (b) and (c) $L_g = 800\mu$H.

than that when the unit CVF method is used. The dynamic process of the current step is also shown in Fig. 18 (c). Compared with Fig. 17 (c), the oscillation of the capacitor voltage v_{C_ab} at current step is significantly smaller than that of the unit CVF method, so the proposed HPF CVF can improve the dynamic performance of the ICF control, especially under a large L_g.

VII. CONCLUSION

This paper has proposed a novel inverter-side current control method of the *LCL*-filtered grid-tied inverter by adding a HPF into the feedforward loop of the *LCL* capacitor voltage. This method is very simple to implement, and can improve the dynamic performance and the grid voltage harmonic attenuation capability of the ICF control. Finally, the effect of the proposed method is verified by the experiment results based on a grid-tied inverter prototype.

APPENDIX

An optimal HPF parameter design method is provided in this section.

According to the feedback control theory, the poles of the closed-loop transfer function can most directly reflect the stability of the system. So the first thing is to obtain the expression of the closed-loop transfer function $T_{cl}(z)$ of the ICF control. From (5) to (9), the complete expression of $T_{cl}(z)$ can be expressed by (A1), where the current controller $G_c(z)$ can be defined as a constant K_c.

$$\begin{aligned} T_{cl}(z) &= \frac{N}{D} \\ N &= T_s K_c \left(z^2 - 2z\cos(\omega_{res}T_s)+1\right) \\ &\quad \times ((\omega_c T_s+2)z+(\omega_c T_s-2)) \\ &\quad + \frac{L_T K_c \sin(\omega_{res}T_s)}{\omega_{res}L_1} \cdot (z-1)^2 \\ &\quad \times ((\omega_c T_s+2)z+(\omega_c T_s-2)) \\ D &= (z^2-z)(L_1+L_T)\left(z^2 - 2z\cos(\omega_{res}T_s)+1\right) \\ &\quad \times ((\omega_c T_s+2)z+(\omega_c T_s-2)) \\ &\quad - 2HL_T[1-\cos(\omega_{res}T_s)](z-1)^2(z+1)+N \end{aligned} \tag{A1}$$

In (A1), it is very difficult to express the poles of $T_{cl}(z)$ with an accurate formula by solving $D = 0$. However, with the help of computers, we can get the numerical solution of the poles under different conditions. Next an optimal HPF parameter design method based on MATLAB program will be introduced.

The parameter design of the HPF is not a simple single-objective optimization problem, but a trade-off between two goals. In this paper, the HPF is added in the CVF path to achieve two goals at the same time: ensuring proper damping of the *LCL* filter at the resonant frequency and avoiding low-frequency oscillation of the ICF control under weak grids, so that the parameter design of the HPF needs to consider both aspects. However, these two goals are usually conflicting. For example, as shown in Fig. 5, it can be seen that when the value of H is large, the damping effect of the *LCL* filter at the resonant frequency is good, but the risk of low-frequency oscillation under weak grids is increasing; when the value of H is small, the situation is reversed. So it is necessary to define an evaluation function that can reflect both goals.

In Fig. 5, it can be seen that there are always 5 poles of the closed-loop transfer function for the ICF control with HPF CVF, regardless the value of the grid inductance or the parameters of the HPF (this conclusion can be proved by (A1), because the highest order of z in the denominator of $T_{cl}(z)$ is 5th). Generally, in discrete domain analysis, if the pole of the closed-loop transfer function is closer to the origin (0, 0), the more stable the entire control system is. Therefore, we can define the sum of the distances of all poles of the closed-loop transfer function from the origin as a sign of judging the stability of a closed-loop control system. However, it should be noticed that the farther a pole is from the origin, the more it affects system stability. In order to select the optimal parameters of the HPF more effectively, we need

to weight the distance from the pole to the origin rather than simply using the actual distance from the pole to the origin. For example, if the actual distance from the pole to the origin is D_x, the weighted distance D_{xw} can be expressed as (A2).

$$D_{xw} = D_x \cdot 10^{D_x} \tag{A2}$$

The plot of (A2) is shown in Fig. 19, where D_x increases from 0 to 1. From Fig. 19, it can be seen that when the actual distance D_x is larger, the weighted distance D_{xw} increases faster.

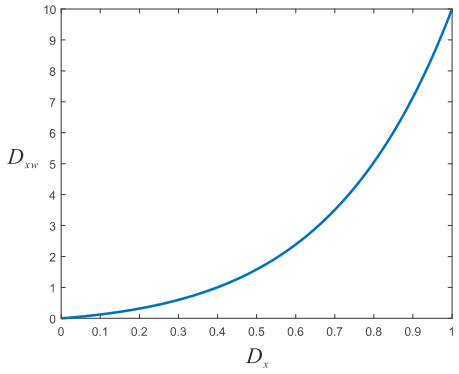

FIGURE 19. The relationship curve between D_x and D_{xw}.

So, the stability of $T_{cl}(z)$ can be defined quantitatively by the evaluation function (EF) as shown in (A3). The value of the evaluation function represents the sum of the 5 weighted distances from all poles of the closed-loop transfer function $T_{cl}(z)$ to the origin.

$$EF = \sum_{x=1,2,3,4,5} D_x \cdot 10^{D_x} \tag{A3}$$

Besides, the changes of the grid inductance L_g should also be taken into account. From Fig. 5, it is obvious that on the one hand, when the grid inductance $L_g = 0\mu$H, the damping of the *LCL* filter at the resonant frequency is weak, but with the increase of L_g, the damping of the *LCL* filter becomes better; on the other hand, when the grid inductance $L_g = 0\mu$H, the risk of low-frequency oscillation is low, but with the increase of L_g, the risk of low-frequency oscillation gets higher. So, the minimum and maximum values of L_g must be considered during the design process of the HPF parameters. With that in mind, the final expression of the evaluation function should be defined as (A4).

$$EF_{\_final} = \frac{EF(L_g = \min) + EF(L_g = \max)}{2} \tag{A4}$$

Therefore, an optimal HPF parameter design method can be described as: constantly changing the value of the HPF parameters, and calculating the $EF_{\_final}$ values under different HPF parameters, and then comparing the $EF_{\_final}$ values to find out the minimum value of $EF_{\_final}$, and selecting the HPF parameters corresponding to the minimum $EF_{\_final}$ value as the optimal parameters. Based on the simulation and experiment parameters above, a matlab program example of is shown as follows.

```
Fs=12000;%control frequency
Ts=1/Fs;
z=tf('z',Ts);
Cf=30e-6;
L1=400e-6;
L2=190e-6;
Kc=1.85;
wc=2*pi*1000;
EFfinal=1000;%initial value of EF
Hfinal=0;%initial value of H
for H=0:0.01:1;
Lg=0e-6;%Lgmin
LT=L2+Lg;
wres=sqrt((L1+LT)/(L1*LT*Cf));
A=(z^2-2*z*cos(wres*Ts)+1);
B=((wc*Ts+2)*z+(wc*Ts-2)); N=(Ts*Kc*A*B+LT
*Kc*sin(wres*Ts)/wres/L1*(z-1)^2*B);
D=(z*(z-1)*(L1+LT)*A*B-2*H*LT*(1-cos(wres*Ts))
*(z-1)^2*(z+1)+N);
Tcl=N/D;
Pmin=pole(Tcl);
Dmin=sum(abs(Pmin)); EFmin=sum(abs(Pmin).
*10.^(abs(Pmin)));
Lg=800e-6;%Lgmax
LT=L2+Lg;
wres=sqrt((L1+LT)/(L1*LT*Cf));
A=(z^2-2*z*cos(wres*Ts)+1);
B=((wc*Ts+2)*z+(wc*Ts-2));
N=(Ts*Kc*A*B+LT*Kc*sin(wres*Ts)
/wres/L1*(z-1)^2*B);
D=(z*(z-1)*(L1+LT)*A*B-2*H*LT
*(1-cos(wres*Ts))*(z-1)^2*(z+1)+N);
Tcl=N/D;
Pmax=pole(Tcl);
Dmax=sum(abs(Pmax));
EFmax=sum(abs(Pmax). *10.^(abs(Pmax))
);
EF=(EFmin+EFmax)/2;
if EF<EFfinal
    EFfinal=EF;
    Hfinal=H;
end
end
```

By running the above MATLAB program, the optimal value of H can be selected as 0.47 (represented by "Hfinal" in the MATLAB program) under the condition of $\omega_c = 6280$ rad/s, which is very close to the value ($H = 0.5$) obtained by comparing the MATLAB plots in Fig. 5. Certainly, if the result is not satisfactory, we can also continue to change the value of ω_c to find more suitable ω_c and H as the HPF parameters.

REFERENCES

[1] W. Wu, Y. Liu, Y. He, H. S.-H. Chung, M. Liserre, and F. Blaabjerg, "Damping methods for resonances caused by LCL-filter-based current-controlled grid-tied power inverters: An overview," *IEEE Trans. Ind. Electron.*, vol. 64, no. 9, pp. 7402–7413, Sep. 2017.

[2] E. Twining and D. Holmes, "Grid current regulation of a three-phase voltage source inverter with an LCL input filter," *IEEE Trans. Power Electron.*, vol. 18, no. 3, pp. 888–895, May. 2003.

[3] M. Liserre, F. Blaabjerg, and S. Hansen, "Design and control of an LCL-filter-based three-phase active rectifier," *IEEE Trans. Ind. Appl.*, vol. 41, no. 5, pp. 1281–1291, Sep. 2005.

[4] X. Wang, F. Blaabjerg, and P. C. Loh, "Grid-current-feedback active damping for LCL resonance in grid-connected voltage-source converters," *IEEE Trans. Power Electron.*, vol. 31, no. 1, pp. 213–223, Jan. 2016.

[5] J. Xu, S. Xie, and T. Tang, "Active damping-based control for grid-connected *LCL*-filtered inverter with injected grid current feedback only," *IEEE Trans. Ind. Electron.*, vol. 61, no. 9, pp. 4746–4758, Sep. 2014.

[6] Z. Xin, X. Wang, P. C. Loh, and F. Blaabjerg, "Grid-current-feedback control for LCL-filtered grid converters with enhanced stability," *IEEE Trans. Power Electron.*, vol. 32, no. 4, pp. 3216–3228, Apr. 2017.

[7] Y. Tang, P. C. Loh, P. Wang, F. H. Choo, and F. Gao, "Exploring inherent damping characteristic of LCL-filters for three-phase grid-connected voltage source inverters," *IEEE Trans. Power Electron.*, vol. 27, no. 3, pp. 1433–1443, Mar. 2012.

[8] C. Zou, B. Liu, S. Duan, and R. Li, "Influence of delay on system stability and delay optimization of grid-connected inverters with LCL filter," *IEEE Trans. Ind. Informat.*, vol. 10, no. 3, pp. 1775–1784, Aug. 2014.

[9] J. Wang, J. D. Yan, L. Jiang, and J. Zou, "Delay-dependent stability of single-loop controlled grid-connected inverters with LCL filters," *IEEE Trans. Power Electron.*, vol. 31, no. 1, pp. 743–757, Jan. 2016.

[10] C. Zou, B. Liu, S. Duan, and R. Li, "A feedfoward scheme to improve system stability in grid-connected inverter with LCL filter," in *Proc. IEEE Energy Convers. Congr. Expo.*, Denver, CO, USA, Sep. 2013, pp. 4476–4480.

[11] C. Citro, P. Siano, and C. Cecati, "Designing inverters' current controllers with resonance frequencies cancellation," *IEEE Trans. Ind. Electron.*, vol. 63, no. 5, pp. 3072–3080, May 2016.

[12] A. Akhavan, H. R. Mohammadi, J. C. Vasquez, and J. M. Guerrero, "Passivity-based design of plug-and-play current-controlled grid-connected inverters," *IEEE Trans. Power Electron.*, vol. 35, no. 2, pp. 2135–2150, Feb. 2020.

[13] Y. He, K.-W. Wang, and H. S.-H. Chung, "Utilization of proportional filter capacitor voltage feedforward to realize active damping for digitally-controlled grid-tied inverter operating under wide grid impedance variation," in *Proc. IEEE Energy Convers. Congr. Expo. (ECCE)*, Sep. 2014, pp. 4450–4457.

[14] M. Lu, A. Al-Durra, S. M. Muyeen, S. Leng, P. C. Loh, and F. Blaabjerg, "Benchmarking of stability and robustness against grid impedance variation for LCL-filtered grid-interfacing inverters," *IEEE Trans. Power Electron.*, vol. 33, no. 10, pp. 9033–9046, Oct. 2018.

[15] J. Jo, H. An, and H. Cha, "Stability improvement of current control by voltage feedforward considering a large synchronous inductance of a diesel generator," *IEEE Trans. Ind. Appl.*, vol. 54, no. 5, pp. 5134–5142, Sep. 2018.

[16] J. Wang, Y. Song, and A. Monti, "A study of feedforward control on stability of grid-parallel inverter with various grid impedance," in *Proc. IEEE 5th Int. Symp. Power Electron. Distrib. Gener. Syst.*, Galway, Ireland, Jun. 2014, pp. 1–8.

[17] J. Xu, T. Tang, and S. Xie, "Evaluations of current control in weak grid case for grid-connected LCL-filtered inverter," *IET Power Electron.*, vol. 6, no. 2, pp. 227–234, Feb. 2013.

[18] M. Lu, X. Wang, F. Blaabjerg, S. M. Muyeen, A. Al-Durra, and S. Leng, "Grid-voltage-feedforward active damping for grid-connected inverter with LCL filter," in *Proc. IEEE Appl. Power Electron. Conf.*, Long Beach, CA, USA, Mar. 2016, pp. 1941–1946.

[19] R. Zhao, Q. Li, H. Xu, Y. Wang, and J. M. Guerrero, "Harmonic current suppression strategy for grid-connected PWM converters with LCL filters," *IEEE Access*, vol. 7, pp. 16264–16273, 2019.

[20] T. Abeyasekera, C. Johnson, D. Atkinson, and M. Armstrong, "Suppression of line voltage related distortion in current controlled grid connected inverters," *IEEE Trans. Power Electron.*, vol. 20, no. 6, pp. 1393–1401, Nov. 2005.

[21] Z. Xin, P. Mattavelli, W. Yao, Y. Yang, F. Blaabjerg, and P. C. Loh, "Mitigation of grid-current distortion for LCL-filtered voltage-source inverter with inverter-current feedback control," *IEEE Trans. Power Electron.*, vol. 33, no. 7, pp. 6248–6261, Jul. 2018.

[22] Q. Yan, X. Wu, X. Yuan, and Y. Geng, "An improved grid-voltage feedforward strategy for high-power three-phase grid-connected inverters based on the simplified repetitive predictor," *IEEE Trans. Power Electron.*, vol. 31, no. 5, pp. 3880–3897, May. 2016.

[23] J. Xu, B. Zhang, L. Xiao, Q. Qian, and S. Xie, "Improved inverter-side current control for grid-connected ZCZ-filtered inverter with low grid current distortion and high robustness," in *Proc. IEEE Southern Power Electron. Conf.*, Puerto Varas, Chile, Dec. 2017, pp. 1–6.

[24] Q. Qian, S. Xie, L. Huang, J. Xu, Z. Zhang, and B. Zhang, "Harmonic suppression and stability enhancement for parallel multiple grid-connected inverters based on passive inverter output impedance," *IEEE Trans. Ind. Electron.*, vol. 64, no. 9, pp. 7587–7598, Sep. 2017.

[25] G. F. Franklin, J. D. Powell, and A. Emami-Naeini, "Digital control," in *Feedback Control of Dynamic Systems*, 6th ed. Upper Saddle River, NJ, USA: Pearson Educ., 2009, ch. 8, pp. 603–604.

[26] P. Rodriguez, J. Pou, J. Bergas, J. I. Candela, R. P. Burgos, and D. Boroyevich, "Decoupled double synchronous reference frame PLL for power converters control," *IEEE Trans. Power Electron.*, vol. 22, no. 2, pp. 584–592, Mar. 2007.

XINGDA ZHOU (Student Member, IEEE) was born in Jiangsu, China, in 1994. He received the B.S. degree in electrical engineering from Chongqing University, Chongqing, China, in 2015, where he is currently pursuing the Ph.D. degree in electrical engineering.

His current research interests include LCL filter active damping technology, three-level inverters, and arc-suppression power electronic equipment in distribution networks.

SHUAI LU (Member, IEEE) received the B.S.E.E. degree from Chongqing University, Chongqing, China, in 1997, the M.S.E.E. degree from the University of Wisconsin, Milwaukee, USA, in 2003, and the Ph.D. degree in electrical engineering from the University of Missouri–Rolla, Rolla, USA, in 2007.

In February 2007, he joined MTS Systems Corporation, Eden Prairie, MN, USA, where he was the lead power electronics and motor drive engineer for the successful development of the world's first generation of the hybrid electric system for Formula-1 cars in the 2009 race season (also known as KERS: Kinetic Energy Recovery System), which is arguably the highest power density and performance hybrid electric system in the world. In the late 2012, he joined Chongqing University as a Professor, where he has established seven laboratories (two of them are multimegawatts rating test systems) and accomplished numerous industrial Research and Development projects in various areas of power electronics and motor drives with the particular focus on the applications in hybrid and electric vehicles, and renewable energy systems. During his Ph.D. research, he authored or coauthored 20 technical articles, including seven IEEE TRANSACTIONS articles.